Transition prediction in hypersonic regime on complex geometries with RANS-based models

L. Cutrone*, A. Schettino†
CIRA, Centro Italiano Ricerche Aerospaziali, Capua, CE, Italy, 81043

José I. Cardesa‡, Grégory Delattre§
ONERA / DMPE, Université de Toulouse, F-31055, Toulouse, France

James G. Coder¶, Steven Qiang‖
Pennsylvania State University, University Park, PA 16802, U.S.A.

E. Vogel**, M. Choudhari††
NASA Langley Research Center, Hampton, VA, 23681, U.S.A.

In the near future, RANS computations will continue to play a significant role in the design of hypersonic vehicles with complex geometries. Therefore, it is imperative to continue testing, benchmarking, and refining the RANS models. In the present study, we evaluate RANS-like, transport equations-based models for predicting laminar-turbulent transition over a full-scale scale model of the BOLT flight configuration that was tested in the CUBRC LENS-II wind tunnel test facility. Based on the availability of the experimental results, comparisons are made between computations from several pre-existing transition models and Computational Fluid Dynamics (CFD) codes, with an emphasis on using the same computational meshes and flow conditions for all computations. The analysis covers the sensitivity of the transition predictions to the input parameters for five different transition models (four mainstream models designed for low-speed flows and a uniquely high-speed model), grid resolution, and the details of model implementation across three different flow solvers. The results show that the phenomenological models can describe significant aspects of the measured transition front. However, a number of additional improvements are required before these models can offer more reliable estimates of transition in high-speed flows.

I. Nomenclature

d_w	=	Wall distance, m
He	=	Helicity, s
k	=	Turbulent kinetic energy, m^2/s^2
Ma	=	Mach number
Re$_V$	=	Vorticity-based Reynolds number
$\tilde{\text{Re}}_\theta$	=	Local transition onset momentum-thickness Reynolds number
Re$_{\theta_c}$	=	Critical momentum-thickness Reynolds number
S	=	Distance from the primary surface symmetry to the lateral surface symmetry, m
Tu	=	Turbulence intensity level
U	=	Velocity magnitude, m/s

*Senior researcher, Aerothermodynamics Department, via Maiorise snc, Senior member AIAA

†Senior researcher, Aerothermodynamics Department., via Maiorise snc.

‡Senior researcher, Multi-Physics for Energetics Department, 2 Av. Edouard Belin, FR-31055 TOULOUSE CEDEX 4, France.

§Senior researcher, Multi-Physics for Energetics Department, 2 Av. Edouard Belin, FR-31055 TOULOUSE CEDEX 4, France.

¶Associate Professor, Department of Aerospace Engineering, 229 Hammond Bldg, Associate Fellow AIAA.

‖Graduate Research Assistant, Department of Aerospace Engineering, 229 Hammond Bldg

**Research Scientist, Computational AeroSciences Branch, Member AIAA

††Senior Research Scientist, Computational AeroSciences Branch, Fellow AIAA.

V	=	Wall normal velocity, m/s
γ	=	Intermittency
λ_θ	=	Pressure gradient parameter
ω	=	Specific dissipation rate, 1/s
$\vec{\omega}$	=	Vorticity vector, 1/s
Ω	=	vorticity magnitude, 1/s

Subscripts

e	=	boundary layer edge
L	=	local

II. Introduction

Accurate modeling of Boundary Layer Transition (BLT) will be important for the success of future "Apollo" or "Shuttle"-like spacecraft programs and other concepts based on air-breathing propulsion. Since transition to turbulence in a hypersonic boundary layer can amplify the local surface heating by a factor in excess of five with respect to laminar conditions, the process of selecting and sizing the Thermal Protection System (TPS) becomes highly dependent upon the state of the boundary layer. Therefore, using suitable modeling strategies at several levels of the design process can drastically improve our ability to converge toward disruptive, novel designs.

Because of the intricate interactions between several components that impact the transition process, including freestream disturbances and surface roughness, pressure gradients and surface temperature, it is difficult to effectively capture the transitional flows encountered in aerospace applications. RANS computations, while inherently limited in their capability to fully resolve the complex flow physics, strike a balance between computational accuracy and cost-effectiveness. As a result, they are an essential tool for the design and analysis of hypersonic vehicles. However, given the inherent variety as well as the complexity of the transition mechanisms in hypersonic flows, integrating them all into a single transition model remains an ongoing, yet potentially elusive pursuit.

To tackle the challenge of transition prediction using a RANS-like approach, Langtry and Menter introduced the innovative framework of local correlation-based transition modeling (LCTM). Unlike the conventional approach of directly modeling the underlying physical mechanisms, LCTM incorporates meticulously derived correlations in terms of locally constructed quantities into RANS-like transport equations. This unique characteristic enables the framework to effectively accommodate and incorporate a diverse array of transition mechanisms, enhancing its overall predictive capabilities, albeit in an empirical manner. Examples of mainstream models of this type include the well-known models developed by Menter, which are based on the solution of one or more differential equations [1, 2] or even on a fully algebraic framework[3, 4]. More recently, extensions targeting the hypersonic flow regime have been developed[5, 6]. Another prominent model type is the Amplification Factor Transport (AFT) model developed originally by Coder and Maughmer [7] for low-speed streamwise instabilities and more recently extended by Carnes and Coder [8] for crossflow transition. The AFT model is fully compatible with RANS solvers, but has only been partially explored for hypersonic flows [9]. In all of these cases, a large number of constants is required to tune the model performance to a wide range of test cases.

This paper will assess the performance of several of these RANS-based transition models for a three-dimensional configuration that is representative of the forebody of a hypersonic vehicle. The aim is to evaluate the prediction capabilities of different models for a geometry where multiple transition mechanisms may coexist. The configuration selected herein is the one being used for the International BOundary Layer Transition (BOLT) series of Flight Experiments, which was specifically designed to have multiple instability mechanisms that may interact with each other. The geometry was extensively tested in several wind tunnels, including full-scale tests at the CUBRC LENS II wind tunnel[10].

Three different codes will be used, CEDRE[11], a code developed in-house by ONERA, the commercial code Ansys® FLUENT®[12] developed by Ansys Inc. and used by CIRA, and the NASA OVERFLOW [13] code adopted for the computations at the NASA and the Pennsylvania State University. The predictions based on these three solvers will be compared on a common experimental test case from a specific run at CUBRC. A special emphasis is placed on adopting, as far as possible, the same freestream boundary conditions, the same computational mesh, and the same transition models. The sensitivity to freestream boundary conditions, mesh convergence, and particular model features will then be thoroughly analyzed, either by comparing multiple codes at once or by concentrating on a single code.

III. Model Description

A. Local-Correlation Transition Models

RANS-coupled transition models are often associated with an intermittency transport equation, such as the one initially formulated by Suzen et al. [14], or a more complex formulation as that proposed by Steelant and Dick [15]. The intermittency factor γ represents the relative fraction of time that turbulent spots are present at a given spatial location within the transitional flow. It is therefore a measure of the progress of the transition process from a laminar to a turbulent flow in the boundary layer. The abovementioned models [14, 15], however, rely on non-local information to induce the onset of transition. In 2009, Langtry and Menter [1] introduced a Local Correlation-based Transition Modeling (LCTM) framework to address this issue. Building upon this initial model, several new models were subsequently developed. In this class of models, the transport equation for the intermittency γ is generally formulated as follows:

$$\frac{\partial \rho \gamma}{\partial t} + \frac{\partial (\rho u_j \gamma)}{\partial x_j} = P_\gamma - D_\gamma + \frac{\partial}{\partial x_j} \left[(\mu + \mu_t) \frac{\partial \gamma}{\partial x_j} \right]. \tag{1}$$

where P_γ and E_γ are the production and the destruction terms for γ:

$$P_\gamma = c_{a_1} F_{\text{length}} \rho S \left(\gamma F_{\text{onset}} \right)^{c_b} (1 - \gamma), \quad E_\gamma = c_{a_2} \rho \Omega \gamma F_{\text{turb}} \left(c_{e_2} \gamma - 1 \right). \tag{2}$$

The solution of the above equations relies on a series of calibration coefficients, the values of which depend on the model selection. These values will not be provided in this study; readers are encouraged to refer to the relevant publication for further details.

The intermittency factor γ obtained from Eq. (1) is used to control the production and destruction terms in the turbulent kinetic energy equation of a $k - \omega$ SST turbulence model:

$$\tilde{P}_k = \gamma P_k, \quad \tilde{E}_k = \mathbf{max} \left[\gamma, 0.1 \right] E_k. \tag{3}$$

In addition, the blending function F_1 in the $k - \omega$ SST turbulence model, [16], is modified for transition simulations according to Langtry and Menter [1].

Medida and Badaer [17] suggest that the Spalart-Allmaras turbulence model can be coupled with the intermittency-based model in a similar fashion:

$$\tilde{P}_{\tilde{\nu}} = \gamma_S P_{\tilde{\nu}}, \quad \tilde{E}_{\tilde{\nu}} = \mathbf{max} \left[\gamma_S, 0.1 \right] E_{\tilde{\nu}}, \tag{4}$$

where, $\tilde{P}_{\tilde{\nu}}$ and $\tilde{E}_{\tilde{\nu}}$ are the production and destruction from the original model and $\gamma_S = \frac{\min[\gamma, 1/c_{e_2}]}{1 - 1/c_{e_2}}$.

1. Langtry, Menter 2009 (MODEL-1) [1]

In the Langtry Menter transition model, both F_{onset} and F_{length} are function of the local transition onset momentum-thickness Reynolds number ($\tilde{\text{Re}}_{\theta_t}$) which is obtained by solving a differential equation:

$$\frac{\partial (\rho \tilde{\text{Re}}_{\theta_t})}{\partial t} + \frac{\partial (\rho U_j \tilde{\text{Re}}_{\theta_t})}{\partial x_j} = P_{\theta_t} + \frac{\partial}{\partial x_j} \left[\sigma_{\theta_t} (\mu + \mu_t) \frac{\partial \tilde{\text{Re}}_{\theta_t}}{\partial x_j} \right]. \tag{5}$$

The initial model considers only streamwise transition and is denoted here as MODEL-1A. In 2015, Menter et al. [2] expanded the model to include crossflow transition. This variant, referred here to as MODEL-1B will also be analyzed.

2. Smirnov, Menter 2015 (MODEL-2) [2]

The intermittency transition model proposed by Smirnov and Menter in 2015 [2] is a further development based on the 2009 Langtry and Menter $\gamma - \tilde{\text{Re}}_{\theta_t}$ transition model which solves only one transport equation for the turbulence intermittency and avoids the need for the second differential equation. The model was initially developed to take into account only for streamwise transition but it was later expanded to incorporate crossflow transition as well [18]. The function F_{onset} is here evaluated by taking the maximum value between the streamwise and crossflow contributions, computed as follows:

$$F_{\text{onset}} = \mathbf{max} \left[F_{\text{onset,s}}, F_{\text{onset,CF}} \right],$$

$$F_{\text{onset,s}} = \frac{\text{Re}_V}{2.2 \text{Re}_{\theta_c}}, \quad F_{\text{onset,CF}} = \mathbf{min} \left[\mathbf{max} \left[100 \left(\frac{C_{RSF}}{150} \left(G \Psi \text{Re}_V \right) - 1 \right), 0 \right], 1 \right]. \tag{6}$$

The streamwise triggering function, $F_{\text{onset,s}}$, is determined by an algebraic expression for Re_{θ_c} that depends on the turbulence intensity level, Tu_L and the pressure gradient, λ_{θ_L}, calculated using local variables as follows:

$$Tu_L = \mathbf{min}\left[100\frac{\sqrt{2k/3}}{\omega d_w}, 100\right], \quad \lambda_{\theta_L} = -0.1111\frac{dV}{dy}\frac{d_w^2}{\nu} + 0.1875. \tag{7}$$

The crossflow triggering function, $F_{\text{onset,cf}}$, was instead based on the Arnal's C1 criterion [19]. It is formulated using local variables and maintains Galilean invariance. The crossflow indicator function Ψ is a non-dimensional measure of the local crossflow intensity in relation to the streamwise intensity and it is computed based on the wall normal change of the normalized vorticity vector, $\vec{e}_\omega$, and the distance from closest wall d_w:

$$\Psi = \left|\vec{\phi}\right| d_w, \quad \vec{\phi} = \vec{n} \cdot \nabla \vec{e}_\omega, \quad \vec{e}_\omega = \frac{\vec{\omega}}{|\vec{\omega}|}. \tag{8}$$

The model variant considering only the streamwise correlation will be denoted as MODEL-2A, whereas with the inclusion of both streamwise and crossflow correlations it will be marked as MODEL-2B.

3. Algebraic Model (MODEL-3), [3]

The latest advancement within the LCTM framework, developed by Menter et al. in 2022 [3], is the algebraic transition model. This model introduces a further simplification, allowing the determination of the intermittency factor γ through an algebraic equation, thus obviating the need to solve any differential equations. The intermittency factor is calculated by:

$$\gamma = \tanh\left[\left(\frac{\text{Re}_{V22}}{\text{Re}_{\theta_c}}\right)^2\right], \tag{9}$$

where

$$\text{Re}_{V22} = \mathbf{min}\left[\frac{\tilde{\Omega}d_w^2}{2.2\nu}, 5000\right], \quad \text{Re}_{\theta_c} = g\left(Tu_L, \lambda_{\theta_L}\right), \tag{10}$$

are function of the local turbulence intensity level, Tu_L and the local pressure gradient, λ_{θ_L}. MODEL-3 does not include a crossflow onset function.

4. Hypersonic Transition Model (MODEL-4) [5]

Liu et al. [5] used the LCTM framework to propose a fully local three-equation transition model for hypersonic flows. Their model takes into account different transition mechanisms, including stream-wise instability, nose-bluntness effects, and crossflow-induced transition. Similar to the Menter model, the function F_{onset} is evaluated in this case by determining the maximum value between the streamwise and crossflow contributions, calculated as follows:

$$F_{\text{onset}} = \mathbf{max}\left[F_{\text{onset,s}}, F_{\text{onset,CF}}\right],$$
$$F_{\text{onset,s}} = \frac{\text{Re}_V}{f(\text{Ma}_{eL}, T_{eL})\text{Re}_{\theta_c}}, \quad F_{\text{onset,CF}} = \frac{\Delta H_{\text{CF}}\text{Re}_V}{f(\text{Ma}_{eL}, T_{eL})C_{\text{CF,crit}}}. \tag{11}$$

In the streamwise triggering function, $F_{\text{onset,s}}$, the component $f(\text{Ma}_{eL}, T_e L)$ is based on self-similar boundary layer profiles obtained without pressure gradient. These profiles are parameterized through local estimations of Mach and temperature at the boundary layer's edge. Conversely, the value of Re_{θ_c} is obtained through an algebraic correlation that depends on the local turbulence intensity level Tu_L. The crossflow triggering function is instead based on the concept of local helicity, He, which is dimensionless with respect to wall distance and velocity magnitude, and then increased by the eddy-to-molecular viscosity ratio as:

$$\Delta H_{\text{CF}} = \frac{d_w He}{U}\left(1.0 + \mathbf{min}\left[\frac{\mu_t}{\mu}, 0.3\right]\right). \tag{12}$$

Unlike the crossflow triggering function of MODEL-2B based on the indicator function Ψ, the present triggering function does not feature Galilean invariance. Two versions of the model will be employed, namely MODEL-4A and MODEL-4B, depending on whether only the streamwise correlation or both the streamwise and crossflow correlations are activated, respectively.

Model	References	Variants	Available in:
MODEL-1	Langtry, Menter 2009,[1]	Baseline (A), Crossflow (B)	FLUENT,[1] OVERFLOW
MODEL-2	Smirnov, Menter 2015, [2]	Baseline (A), Crossflow (B)	FLUENT, CEDRE, OVERFLOW[1]
MODEL-3	Menter 2022, [3]	Baseline	FLUENT, CEDRE
MODEL-4	Liu, [5]	Baseline (A), Crossflow (B)	CEDRE, OVERFLOW
MODEL-5	Coder, Maughmer [7, 8]	AFT2019b (A), AFT2019b+CF (B)	OVERFLOW

Table 1   Summary of the adopted transition model nomenclature.

[1] available, but not used in the present work.

B. Amplification Factor Transport (AFT) Transition Model

1. Coder AFT2019b Model (MODEL-5) [7, 8]

The AFT model was originally developed by Coder and Maughmer [7] as a PDE-based realization of the approximate envelope linear-stability method. The specific version used in this study is the AFT2019b model, which is completely described in Ref. [8]. It requires the solution of two auxiliary transport equations: one for the transported amplification factor,

$$\frac{\partial (\rho \tilde{n})}{\partial t} + \frac{\partial (\rho U_j \tilde{n})}{\partial x_j} = \rho \Omega F_{\text{crit}} F_{\text{growth}} \frac{d\tilde{n}}{dRe_\theta} + \frac{\partial}{\partial x_j} \left[\sigma_n (\mu + \mu_t) \frac{\partial \tilde{n}}{\partial x_j} \right],$$

(13)

which effectively tracks the margin to transition and incorporates upstream flow history, and a modified intermittency variable,

$$\frac{\partial (\rho \tilde{\gamma})}{\partial t} + \frac{\partial (\rho U_j \tilde{\gamma})}{\partial x_j} = P_\gamma - E_\gamma + \frac{\partial}{\partial x_j} \left[(\mu + \sigma_\gamma \mu_t) \frac{\partial \tilde{\gamma}}{\partial x_j} \right].$$

(14)

The modified intermittency relates to the standard intermittency variable by the relation $\tilde{\gamma} = \ln \gamma$. This change of variables ensures that transported intermittency is non-negative. In Eq. 13, the function F_{crit} captures the influence of the critical Reynolds number on boundary-layer instability growth. In Eq. 14 the production and destruction terms are calculated in a fashion similar to Eq. 2, with a function F_{onset} which takes into account for both the streamwise and the crossflow transition:

$$F_{\text{onset}} = \mathbf{max} \left[\frac{\tilde{n}}{N_{\text{crit}}}, \frac{\text{Re}_V}{2.2\text{Re}_{\text{SCF}}} \right].$$

(15)

Unlike the LCTM models used in this study, the AFT model is coupled with the one-equation Spalart-Allmaras eddy viscosity model [20] with the Secundov compressibility correction. The AFT model will be labeled MODEL-5A when employing only the streamwise transition function, whereas it will be indicated as MODEL-5B when both the streamwise and crossflow transition functions are applied.

IV. Brief Overview of Flow Solvers

A. Ansys® FLUENT®

Ansys® FLUENT® is a widely used commercial computational fluid dynamics (CFD) software package developed by Ansys, Inc. It is designed for engineers and scientists to simulate and analyze fluid flow, heat transfer, and related phenomena in a variety of industries and applications. Ansys® FLUENT® has been adopted here as a reference solver owing to its integral contribution to the development of several key models, largely attributable to Ansys chief scientist Florian Menter. The extensive integration of these models within the solver is widely acknowledged and regarded as a robust and entrenched practice within the scientific community.

The simulations conducted using Ansys® FLUENT® in this study are carried out using a density-based solver for the turbulent Navier-Stokes equation on unstructured meshes. Numerical fluxes are computed with the AUSM+ [21] approximate Riemann solver and second-order accuracy is obtained by a multidimensional linear reconstruction approach [22], together with a Minmod limiter. The steady-state solutions are obtained by means of the implicit Euler temporal scheme solved using Incomplete Lower Upper factorization (ILU), in conjunction with an algebraic multigrid (AMG) method adapted for coupled sets of equations.

The objective was to explore the impact of the transition model on the distribution of wall heat flux. Two models were examined: the intermittency transition model, both without and with the activation of the crossflow transition

correlation (MODEL-2A and MODEL-2B, respectively), and the algebraic intermittency transition model, (MODEL-3). They have been coupled to the $k - \omega$ SST turbulence model [16].

B. ONERA CEDRE

The multi-physics software suite CEDRE [11] is developed at the French aerospace lab (ONERA) by the Department of Multi-physics for Energetics (DMPE). Within CEDRE, the flow solver CHARME handles the RANS computations of single-phase flows, and transition models have been recently added to it at the ONERA Center of Toulouse to extend its modeling capabilities. CHARME solves governing sets of equations on general unstructured elements through cell-centered finite volume schemes. The present computations rely on a second-order in space, multislope Monotonic Upwind Scheme for Conservation Laws (MUSCL) [23], together with the van Leer limiter. Numerical fluxes are computed with the AUSM+ approximate Riemann solver. The steady-state solutions are obtained by means of the implicit Euler temporal scheme associated to the Generalized Minimal RESidual (GMRES) method. No preconditioning is applied and the number of internal iterations to solve the implicit system is kept fixed at 20 per time step.

The transition models that have been coded in CHARME include MODEL-2A, MODEL-3, MODEL-4A and MODEL-4B. All are coupled to the $k - \omega$ SST turbulence model [16]. The two variants of MODEL-4 are used here without the compressibility or nose bluntness correction terms activated – see the original model for details of these terms [5].

C. NASA OVERFLOW

OVERFLOW is a structured overset RANS solver with a variety of turbulence, transition, and flow modeling options [24]. The software is developed and maintained by NASA Langley Research Center. OVERFLOW has been used for many aerodynamic flow problems, ranging from incompressible flows to the hypersonic regime.

The NASA simulations are performed using a version of OVERFLOW 2.3e that has been modified to include the hypersonic SST-γ model of Liu et al. [5] (MODEL-4). OVERFLOW simulations conducted by NASA participants utilized the HLLE++ upwinded flux scheme with SSOR and the van Albada limiter. These simulations did not utilize QCR, the SST rotational correction, or any turbulence-sustaining terms. The compressibility and nose bluntness corrections provided by Liu et al. [5] are implemented in the OVERFLOW version of the model [25], but were not used in these computations, analogous to the ONERA simulations.

The Pennsylvania State University (PSU) simulations used the OVERFLOW 2.2 version where the AFT (MODEL-5) transition model is coupled to the Spalart Allmaras 1-equation turbulence model.

Computational meshes used in the OVERFLOW simulations are point-matched with the Ansys® FLUENT® and ONERA meshes but split into 4 blocks to satisfy the input requirements of the overset format. More information about overset meshes is provided in Ref. [26].

V. Description of the CUBRC Experiments

The computational test cases in this paper model a specific run from the CUBRC ground facility experiments involving the geometry of the BOLT (BOundary Layer Transition) project, which was designed to investigate the hypersonic boundary layer transition on a low-curvature concave surface with highly swept leading edges seen in Figure 1. A full-scale model of the BOLT geometry underwent extensive ground test experimentation in the LENS-II hypervelocity reflected shock tunnel at CUBRC, and here the conditions of RUN-03 in [10] will be used as reference. These conditions are here briefly summarized: $M = 5.17$, $\mathrm{Re}_L = 3.92 \cdot 10^6$ m^{-1} based on the model's 0.86 m length, with stagnation pressure and temperature equal to 1.5 MPa and 1130 K, respectively. A wall temperature of 294.4 K was imposed. With the usual free-stream noise levels observed to be within the 3-5% span in LENS II[27], the turbulence intensity level at the freestream has been approximated to fall within the 0.42% to 0.7% range, adopting the approach proposed in [28]. However, to better investigate the effects of free-stream turbulence on the transition onset, a broader range was considered for the turbulent intensity in the simulations, selecting four turbulence intensity levels $Tu = 0.1, 0.3, 0.5, 1.0\%$, and three values of the viscosity ratio, $\mu_t/\mu = 1, 5, 10$.

Exploiting both symmetries of the forebody geometry, only one quarter of this geometry was included in the mesh used for the CFD computations. Three shock-fitted structured multi-block meshes with 3.5M, 24M, and 60M cells were created using Ansys® IcemCFD®, and are labeled as GRID-C (coarse), GRID-M (medium), and GRID-F (fine), respectively. These meshes were subsequently converted to the appropriate format for each flow solver.
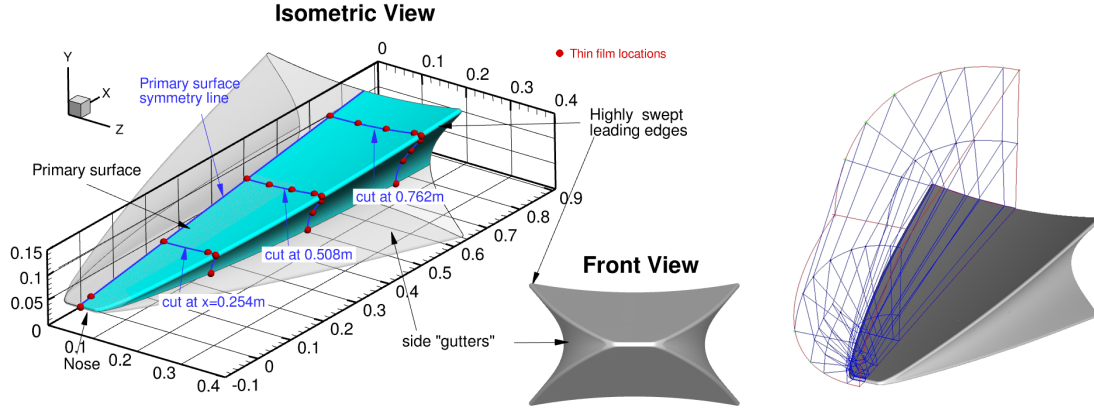
Fig. 1   (left) BOLT geometry, from [10]; (right) domain decomposition for a quarter of the body.

VI. Results - CUBRC

In this section, the comparisons between the numerical results and experimental data are reported. These consist of:
- Wall heat flux contours on the primary surface of the BOLT test article, which are juxtaposed with Thermal Sensitive Paint (TSP) maps to provide a qualitative assessment of the transition front;
- Numerical heat flux profiles compared with Thin Film measurements taken along the primary symmetry lines, and three transverse rows on the surface of the test article.

First, we describe the results derived from each individual solver, with an emphasis on highlighting the sensitivity to the freestream boundary conditions and to the resolution provided by the computational mesh. Following this, we present a comprehensive comparison of the predictions obtained using multiple flow solvers. This comparative study is expected to provide useful insights into the variations in performance and inherent limitations of these transition models as implemented within different computational codes.

A. Ansys® FLUENT® results

1. Mesh resolution sensitivity

Results based on the different transition models are shown in Figure 2. These plots showcase the contours of wall heat flux on the BOLT surface and results are obtained for all three meshes with each of the transition models. It appears that the heat flux has become approximately grid converged with the intermediate grid level (GRID-M), as there are no significant differences between the results on this level and the finest one (GRID-F); for this reason, only the results on this intermediate level will be discussed in all subsequent analyses by CIRA with the Ansys® FLUENT® code.

Comparison of the computed heat flux distributions with the TSP contour map in the top right corner of Figure 2 indicates that all three transition models provide a reasonable alignment with the experiment when the Tu is set at 0.5%. There is no significant difference between the predictions of MODEL-2A and MODEL-2B for this particular free-stream turbulent intensity. However, MODEL-3 systematically predicts an earlier transition than the other two models within the central part of the primary surface (i.e., along the symmetry plane in the simulations). The aforementioned tendency becomes more apparent in Figure 3, which provides a quantitative comparison between the experimental and numerical heat flux profiles. When observing the temperature-sensitive paint (TSP) data on the same graph, it becomes evident that the experiment shows a gradual increase of heat flux and, hence, an extended transition zone spanning approximately 0.3 meters. Conversely, the simulations predict a faster but delayed transition, with MODEL-3 displaying slightly less delay.

2. Free-stream turbulence sensitivity

Figure 4 shows quite clearly the dependence of the transition front position on the free-stream turbulence intensity level enforced at the inlet boundary. It is evident that MODEL-2A and MODEL-3 show a significant dependence of their transition front position on Tu, with a trend towards earlier transition for increasing Tu levels as expected by these models in this kind of applications, [29, 30]: at extremely low Tu levels, both transition models tend to converge towards the laminar solution (not reported here for the sake of brevity). On the other hand, when the correction for cross-flow transition is activated by using MODEL-2B (and BOLT geometry was specifically designed to experience
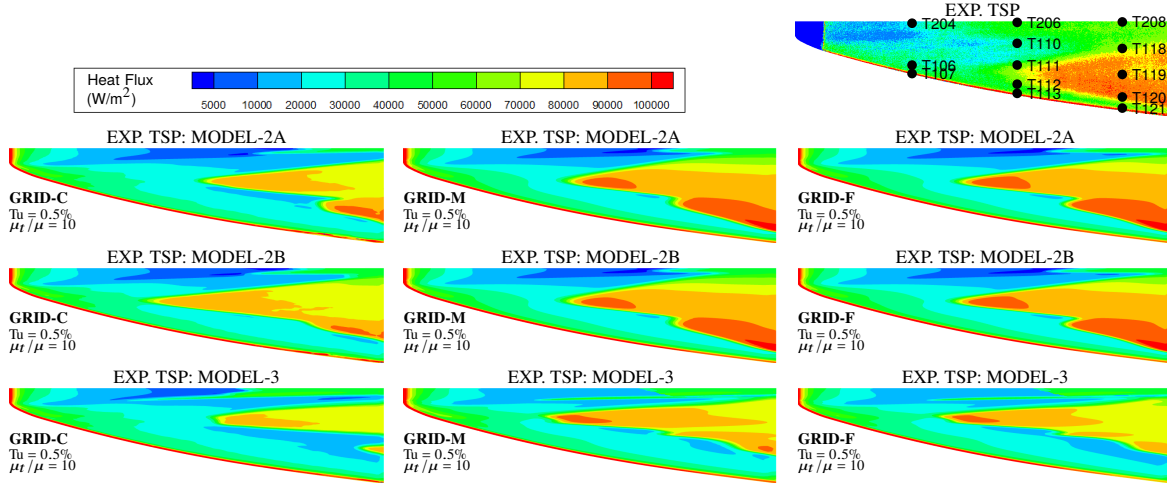
Fig. 2 Ansys® FLUENT® (CIRA): mesh sensitivity analysis, $Tu = 0.5\%$ and $\mu_t/\mu = 10$. Each row corresponds to a specific model and the mesh resolution increases from the left to the right; the measured data from the experiment is plotted on the top right.
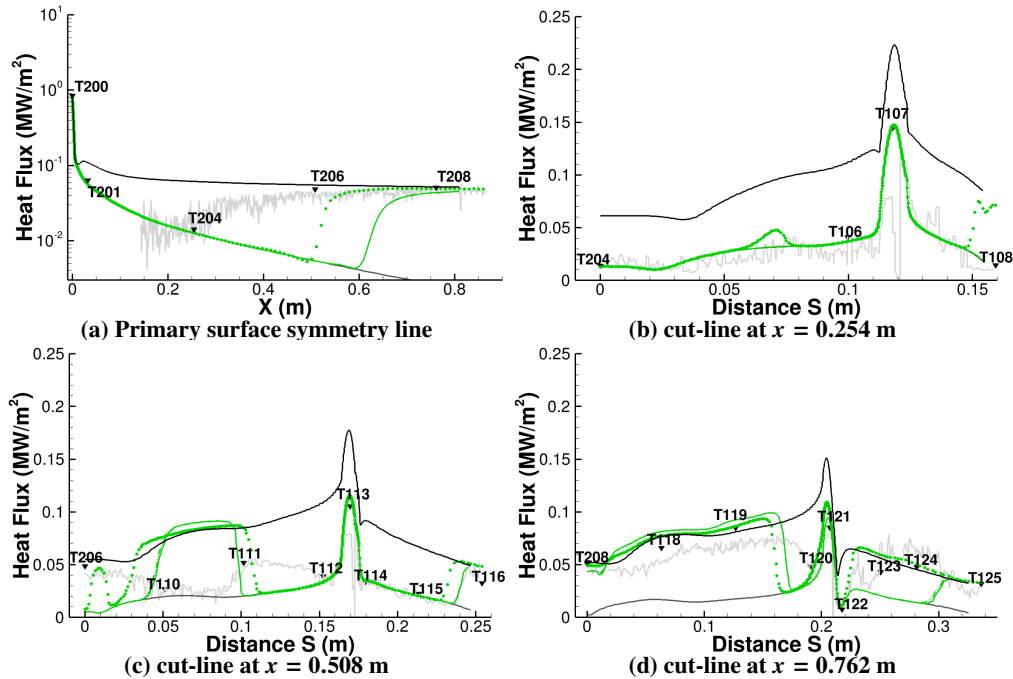

Fig. 3 Ansys® FLUENT® (CIRA): model comparison. Heat flux profiles along the main surface symmetry line and three transverse cut lines. TSP —, Thin films ▼, Turbulent —, Laminar —, MODEL-2A —, MODEL-2B – ·· –, MODEL-3 ···. Turbulence freestream conditions: $Tu = 0.5\%$, $\mu_t/\mu = 10$. GRID-M mesh level. Note that the MODEL-2B results almost match with those from MODEL-2A, thus it is not possible to clearly discern one curve from the other.

this mode of transition) the solutions seem to be less sensitive to the Tu levels, suggesting that crossflow term is entirely responsible for predicting a transition front even at very low Tu levels: only at the highest value considered, $Tu = 1\%$, the streamwise onset terms became predominant and shift significantly forward the transition front.

Figure 5 reports the same sensitivity analysis but this time focusing on the ratio between the eddy and laminar viscosities enforced at the inlet. In contrast to the previous observation, it appears that the transition front based on
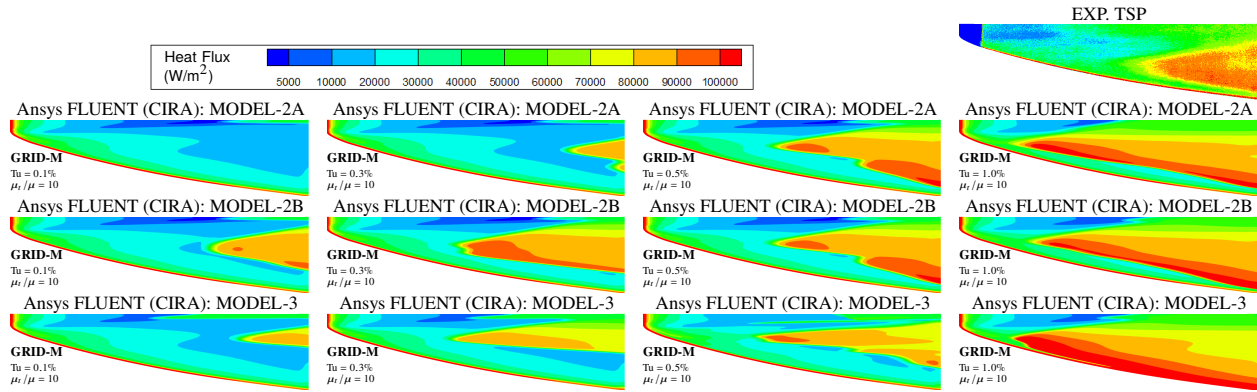
Fig. 4   Ansys® FLUENT® (CIRA): sensitivity to free-stream turbulent intensity level, GRID-M mesh level. Each row corresponds to a specific model and the inflow turbulent intensity increases from the left to the right
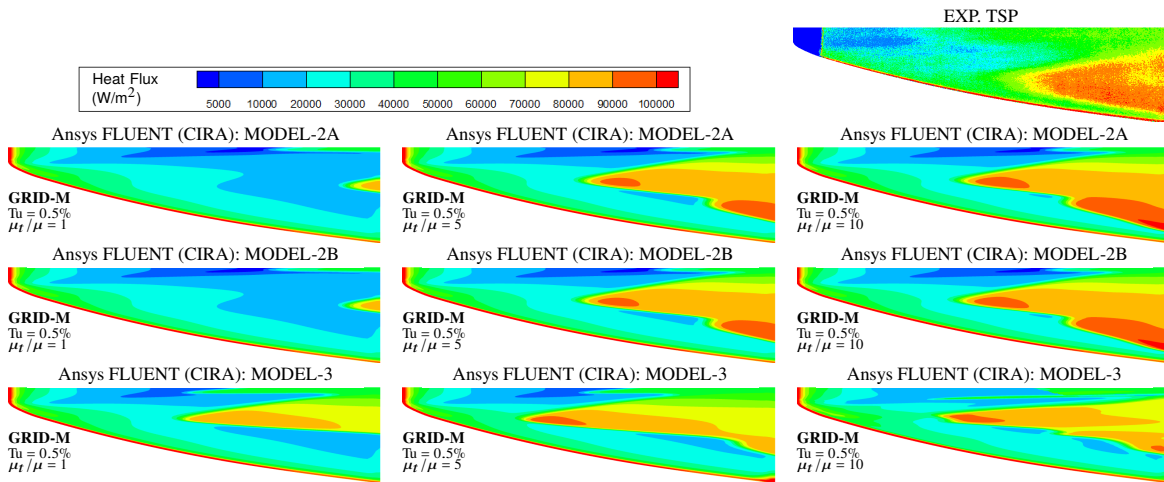
Fig. 5   Ansys® FLUENT® (CIRA): sensitivity to free-stream eddy-to-laminar viscosity ratio, GRID-M mesh level. Each row corresponds to a specific model and the viscosity ratio increases from the left to the right

the wall heat flux is not significantly influenced by this parameter, except for the case when $\mu_t/\mu = 1$: however, it is noteworthy that MODEL-3 appears to be less sensitive with respect to MODEL-2A even for the smaller ratio.

B. ONERA CEDRE Results

1. Mesh resolution sensitivity

The grid convergence studies carried out with CEDRE reveal that differences can still be observed between the heat flux maps obtained with GRID-M and those with GRID-F, as can be seen in Figure 6. A finer grid would be required to confirm that results with GRID-F are indeed converged. However, a general remark can be made on the basis of Figure 6, which is that some models exhibit larger degrees of grid sensitivity than others. For instance, MODEL-2A shows a comparatively lower degree of grid sensitivity between GRID-M and GRID-F than MODEL-3, hinting at the fact that while MODEL-3 may cost one transport equation less, it can require finer grids to converge and hence prove more expensive overall. Another salient feature of insufficient resolution appears to be an early transition in the vicinity of the forebody leading edge, most visible in GRID-C with MODEL-3 and MODEL-4.

Figure 7 shows that at $Tu = 0.3\%$, all transition models exhibit a later transition than that observed experimentally along the primary surface symmetry line, with MODEL-3 predicting the most upstream transition location amongst the four transition models. The cut lines at a constant streamwise location exhibit the correct behavior for the most
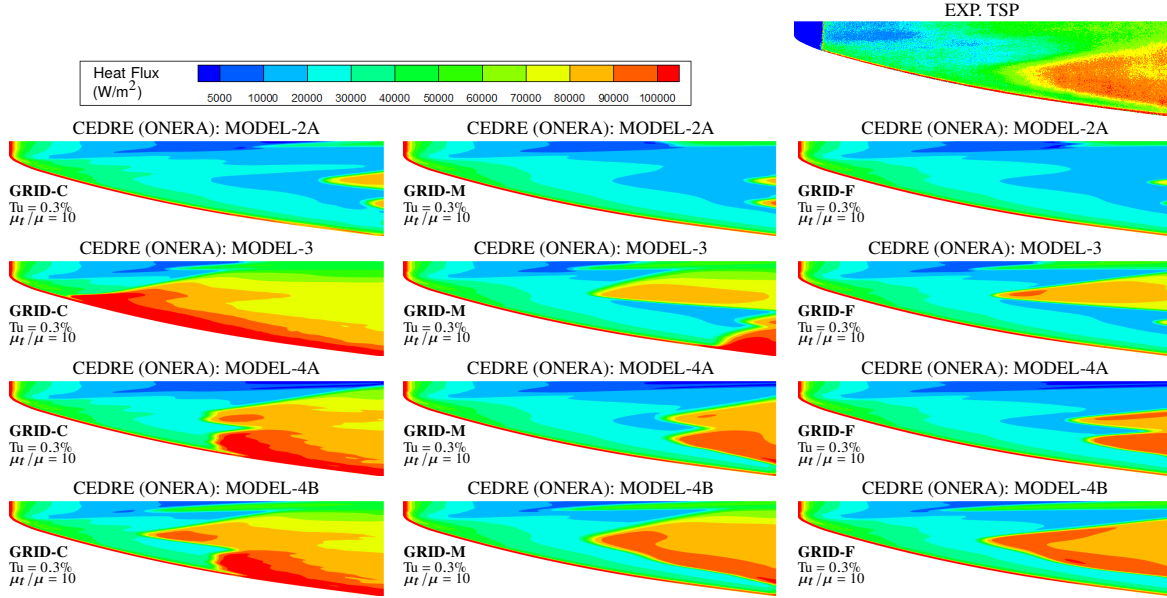
Fig. 6 CEDRE (ONERA): mesh independence analysis, $Tu = 0.3\%$ and $\mu_t/\mu = 10$. Each row corresponds to a specific model and the mesh resolution increases from the left to the right.
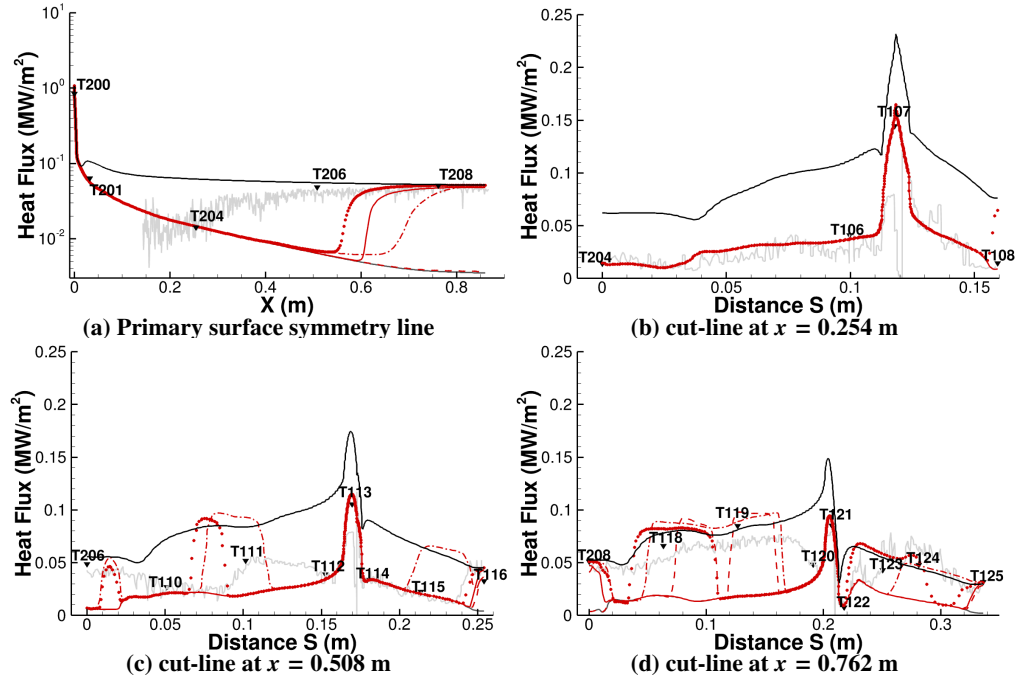

Fig. 7 CEDRE (ONERA): model comparison. Heat flux profiles along the main surface symmetry line and three transverse cut lines. TSP ——, Thin films ▼, Turbulent ——, Laminar ——, MODEL-2A ——, MODEL-3 ·····, MODEL-4A – – –, MODEL-4B –·–. Turbulence freestream conditions: $Tu = 0.3\%$, $\mu_t/\mu = 10$. GRID-F mesh level.

upstream location (fully laminar solutions), while at the two further downstream locations, the complex transition front is reproduced with varying degrees of agreement. MODEL-4A predicts transition the latest. A curious point to note is that MODEL-4A totally fails to predict transition along the primary surface line, while MODEL-2A and MODEL-3 do trigger within the forebody surface. Neither of these three models is designed to capture transition induced by crossflow,
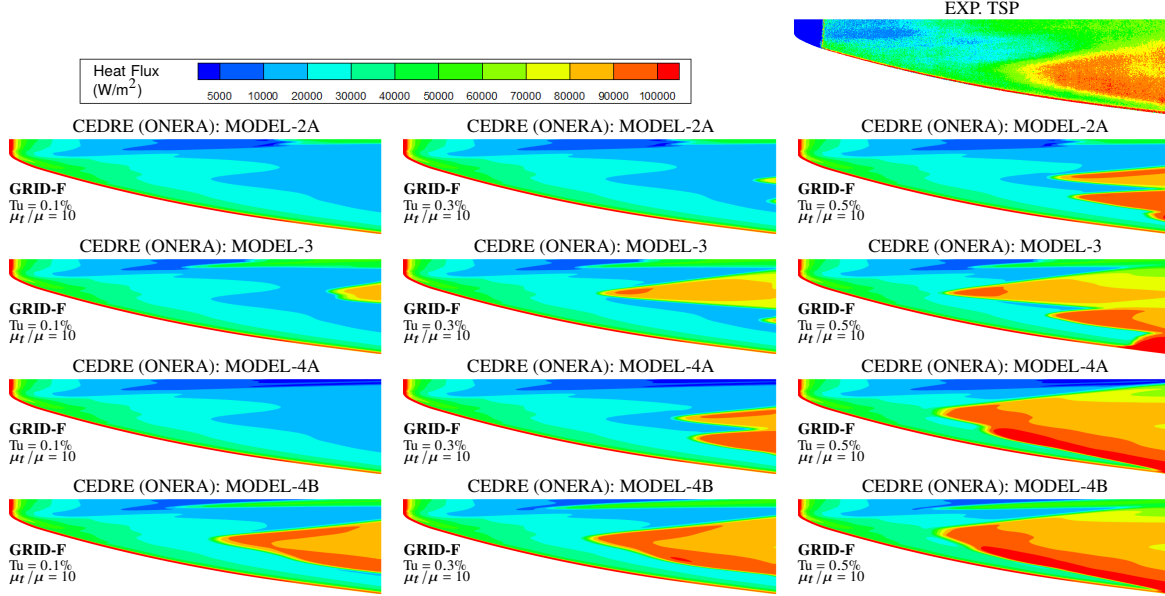
Fig. 8   CEDRE (ONERA) sensitivity to free-stream turbulent intensity level, GRID-F mesh level. Each row corresponds to a specific model and the turbulent intensity increases from the left to the right

according to their developers. So the difference could result from the fact that MODEL-2A and MODEL-3 are calibrated in order to take into account adverse pressure gradient effects. Yet in changing from MODEL-4A to MODEL-4B, no pressure gradient effects are added into the modeling strategy (MODEL-4 stems from self-similar boundary layer profiles obtained without pressure gradient [5]), but the transition along the primary surface line and which is captured by MODEL-2A and MODEL-3 becomes apparent. In conclusion, similar transition results can be arrived at through model correction terms that attribute transition to different mechanisms.

2. Free-stream turbulence sensitivity

The results discussed in the previous section were limited to a single value of freestream Tu. We now look at the effect of this parameter on the transition front location, with results displayed in Figure 8. Overall, the trend is consistent with an earlier transition for increasing freestream Tu. However, other subtle cross-model differences worth highlighting appear at different Tu values. Taking for instance $Tu = 0.1\%$, the differences between MODEL-4A and MODEL-4B are drastic. The difference along the symmetry line (where MODEL-4A predicts fully laminar flow) has already been discussed above. But the area around the mid-span region is where the largest differences are to be found between the two models, and can be entirely attributed to the cross-flow onset term. At $Tu = 0.5\%$, however, both MODEL-4A and MODEL-4B exhibit similar transition fronts in the mid-span region. The only explanation is that the $k-$dependent streamwise onset term in MODEL-4 causes MODEL-4A to transition at $Tu = 0.5\%$, while at $Tu = 0.1\%$ it does not – but the crossflow onset term in MODEL-4B can still trigger at this low k setting. This confirms that similar transition predictions can be arrived at through different onset terms. But even at $Tu = 0.5\%$, MODEL-4A does not show transition along the symmetry line, hinting at the fact that MODEL-2A, MODEL-3 and MODEL-4B all have some feature allowing them to be more accurate than MODEL-4A.

Turning towards MODEL-3, it can be seen that at $Tu = 0.5\%$ a transitional front stemming from the lateral leading edge appears as a "third lobe". This front has been observed to be highly dependent upon grid resolution as its size is considerably larger with GRID-M, and can thus be attributed to a mesh size effect that would most probably disappear with finer meshes.
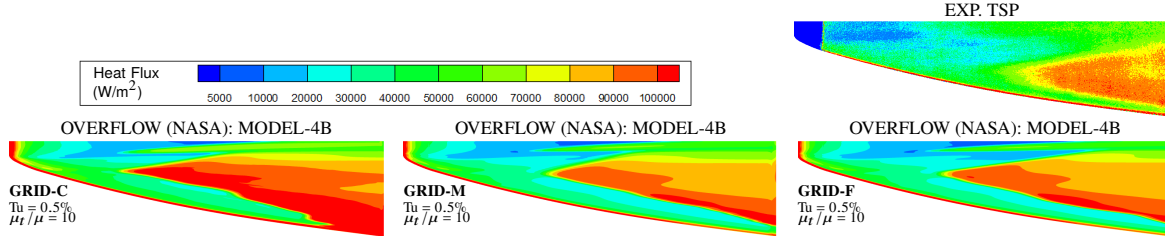
11

Fig. 9 OVERFLOW (NASA): mesh independence analysis, $Tu = 0.5\%$ and $\mu_t/\mu = 10$.
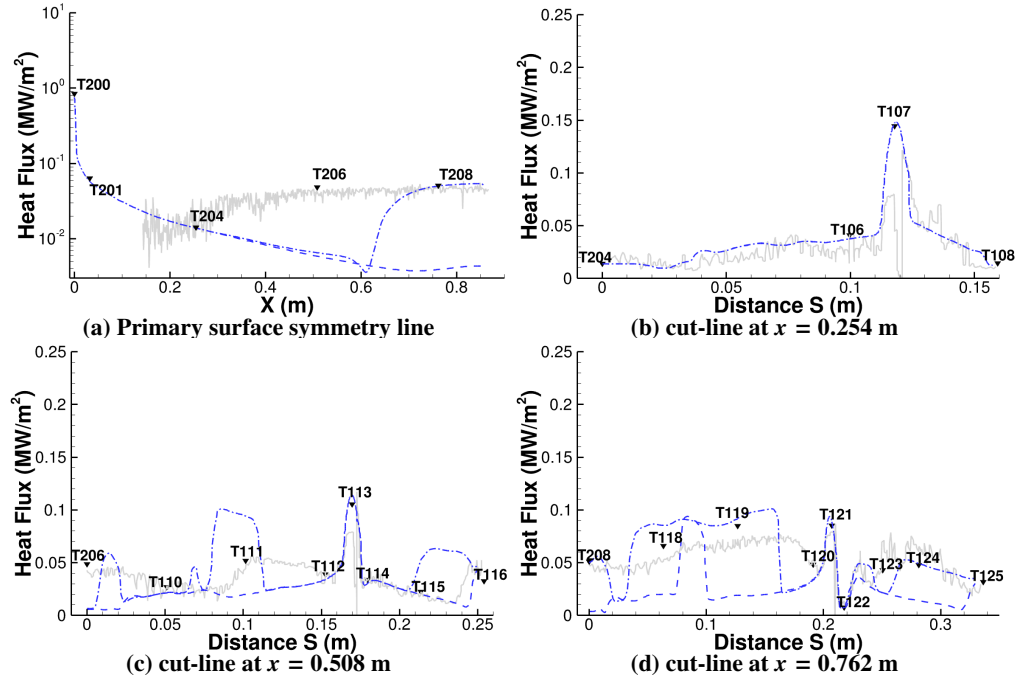

Fig. 10 OVERFLOW (NASA): model comparison. Heat flux profiles along the main surface symmetry line and three transverse cut lines. TSP —, Thin films ▼, MODEL-4A – – –, MODEL-4B –·–. Turbulence inlet conditions: $Tu = 0.5\%$, $\mu_t/\mu = 10$. GRID-F mesh level.

C. NASA-PSU OVERFLOW Results

1. Mesh resolution sensitivity

NASA conducted a mesh sensitivity analysis using the OVERFLOW solver with MODEL-4B by imposing a turbulence intensity level of $Tu = 0.5\%$ at the freestream boundary. The comparison in Figure 9 between the GRID-M and the GRID-F mesh level solutions indicates a comparable transition behavior at the apex of the transition front, whereas a discernible sensitivity is observed in the outboard region, indicating the importance of mesh resolution in capturing detailed flow features. Furthermore, the analysis of the GRID-C mesh level demonstrates a somewhat earlier transition.

The comparisons in Figure 10 emphasize the impact of the crossflow transition correlation on the overall solution, particularly near the symmetry line of the primary test surface. Notably, the MODEL-4A model demonstrates an inability to predict any transition along the symmetry line, even at the highest turbulence intensity level tested, i.e., $Tu = 0.5\%$. Conversely, the results from MODEL-4B exhibit a distinct transition at that location for all three turbulence intensity levels, albeit still delayed in comparison with the measured data.

Concerning the comparison with experimental data, the transition fronts inferred from the wall heat fluxes demonstrate qualitative alignment with the TSP maps for all three grid levels, but suggest an earlier transition for the highest level of freestream turbulent intensity ($Tu = 0.5\%$).

In conjunction with NASA, Pennsylvania State University also conducted simulations using the OVERFLOW solver,

with a specific focus on exploring the capabilities of MODEL-1 and MODEL-5. Notably, in contrast to all the other simulations presented in this study that are based on the Menter SST turbulence model, the MODEL-5 includes a coupling with the Spalart Allmaras 1-equation turbulence model.
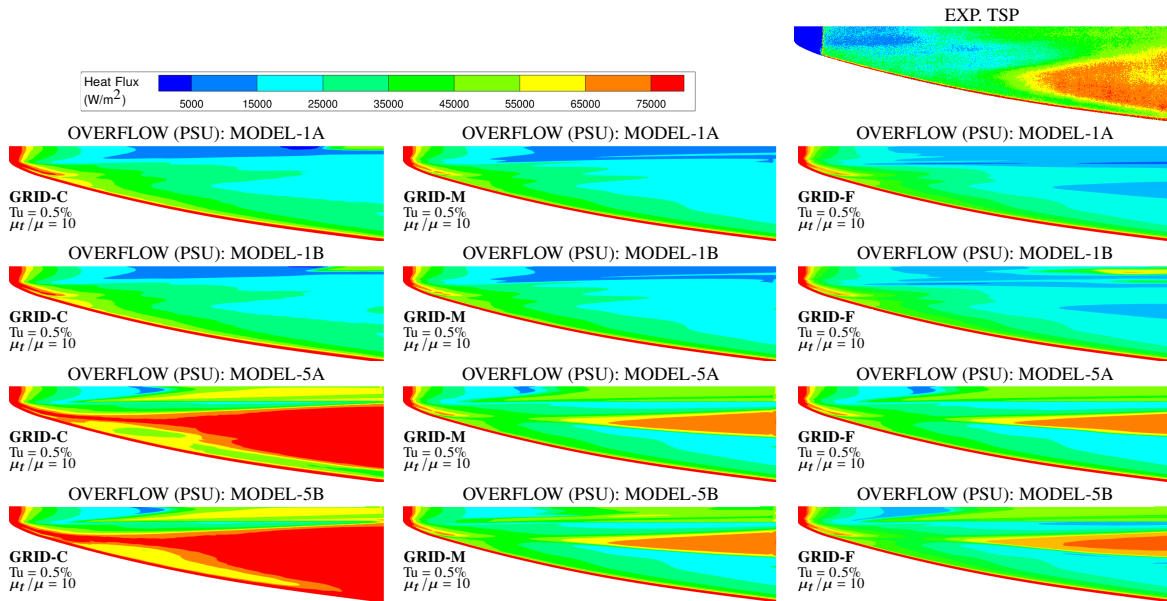

Fig. 11   OVERFLOW (PSU): mesh independence analysis, $Tu = 0.5\%$ and $\mu_t/\mu = 10$.
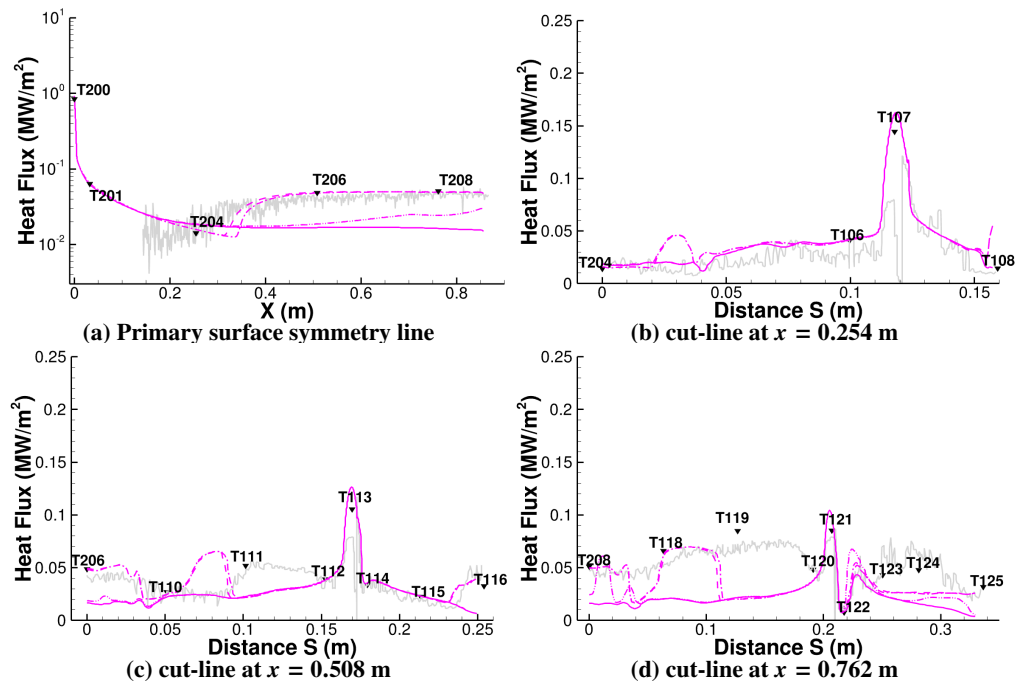

Fig. 12   OVERFLOW (PSU): model comparison. Heat flux profiles along the main surface symmetry line and three transverse cut lines. TSP ——, Thin films ▾, MODEL-1A ——, MODEL-1B –··–, MODEL-5A – – –, MODEL-5B –·–. Turbulence inlet conditions: $Tu = 0.5\%$, $\mu_t/\mu = 10$. GRID-F mesh level.

Figures 11 and 12 depict the comparisons between the numerical wall heat flux and experimental TSP maps, as well as between numerical heat flux profiles and experimental Thin Film measurements. These comparisons are for
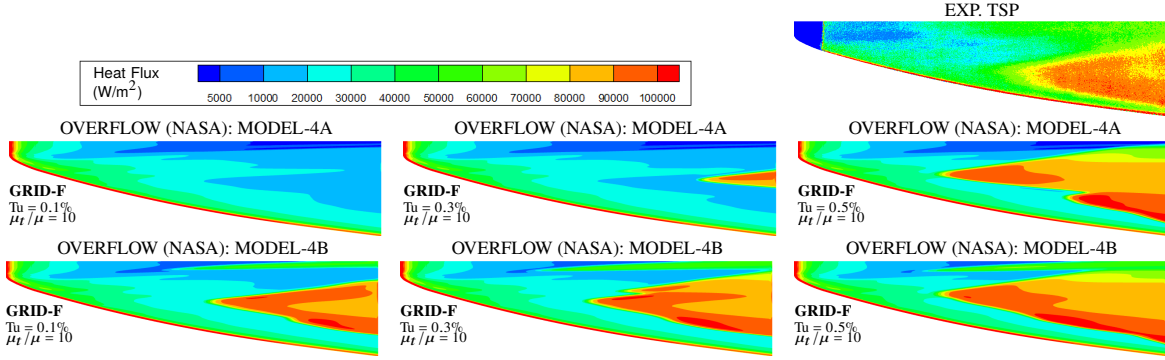
Fig. 13 OVERFLOW (NASA) sensitivity to free-stream turbulent intensity level, GRID-F mesh level. Each row corresponds to a specific model and the turbulent intensity increases from the left to the right

MODEL-1 and MODEL-5, with and without an active crossflow transition correlation. Observations suggest that the crossflow transition correlation plays a small but significant role for both MODEL-1 and MODEL-5. Specifically, when this correlation is inactive, the solutions for MODEL-1A seems akin to the laminar solution, lacking any indications of a transition to turbulence. Conversely, when the crossflow transition is activated, its effect is rather pronounced. MODEL-1B initiates the transition, yet the region of turbulence does not spread across the spanwise extent of the test surface, whereas MODEL-5 exhibits a more pronounced transition front, and at least along the symmetry line. The MODEL-5B exhibits one of the closest agreements with the Thin Film measurements and TSP profile reported in this paper. However, the visually inferred transition front from the wall heat flux on the main surface is narrower compared to the TSP experimental map.

Interestingly, the wall heat flux, as depicted in the contour maps in Figure 11, ranges from 0 to 75,000 W/m^2, closely aligning with the experimental range, unlike the other numerical results presented in this paper where the maximum wall heat flux exceeds the experimental maximum, almost reaching a value of 100,000 W/m^2. This distinction arises from the coupling of MODEL-5 with the SA turbulence model, in contrast to the SST used in the other models, alongside the advantageous effect of a less aggressive transition.

2. Free-stream turbulence sensitivity

NASA carried out a sensitivity analysis to freestream turbulence intensity level for MODEL-4, with and without the crossflow transition correlation activated. The results of this analysis are shown in Fig. 13. Apart from the previously mentioned influence of this modeling option close to the symmetry, the crossflow transition correlation appears to play a significant role in initiating the transition at lower Tu, taking priority over the streamwise transition correlation. Specifically, MODEL-4B predicts a distinct transition front even at $Tu = 0.1\%$. Conversely, MODEL-4A, in accordance with its modeling characteristics, shows strong sensitivity to the Tu level, leading to the downstream shift in the transition front as the freestream turbulence level decreases. Each of these cases achieved a normalized flow variable residual below 1×10^{-9}.

PSU also conducted an analysis of the sensitivity of MODEL-1A, MODEL-1B, MODEL-5A, and MODEL-5B to freestream turbulence intensity, the results of which are shown in Fig. 14. These results show a smaller sensitivity to the crossflow transition terms for MODEL-1 than is observed in the other models examined. Moreover, for the turbulence intensity levels examined ($Tu = 0.1\%$ to $Tu = 0.5\%$), MODEL-1 does not predict transition for most of the streamwise extent of the model with or wihthoug crossflow. For MODEL-5 it is observed that, for the cases where crossflow is active, the transition location is insensitive to Tu, although the contours indicate that the turbulence intensity still impacts the magnitude of the wall heat flux in the turbulent region.

D. Cross-code comparisons

1. Intermittency Transition Model, MODEL-2 (CIRA, ONERA)

Figure 15 shows the comparisons between the MODEL-2A results obtained with the Ansys® FLUENT® solver (CIRA) and the CEDRE solver (ONERA), respectively. These comparisons correspond to the predictions on the finer mesh corresponding to grid level GRID-F and a freestream turbulence level of $Tu = 0.5\%$. Even though both codes demonstrate transition fronts based on the wall heat flux that approximate the experimental TSP map fairly well, notable
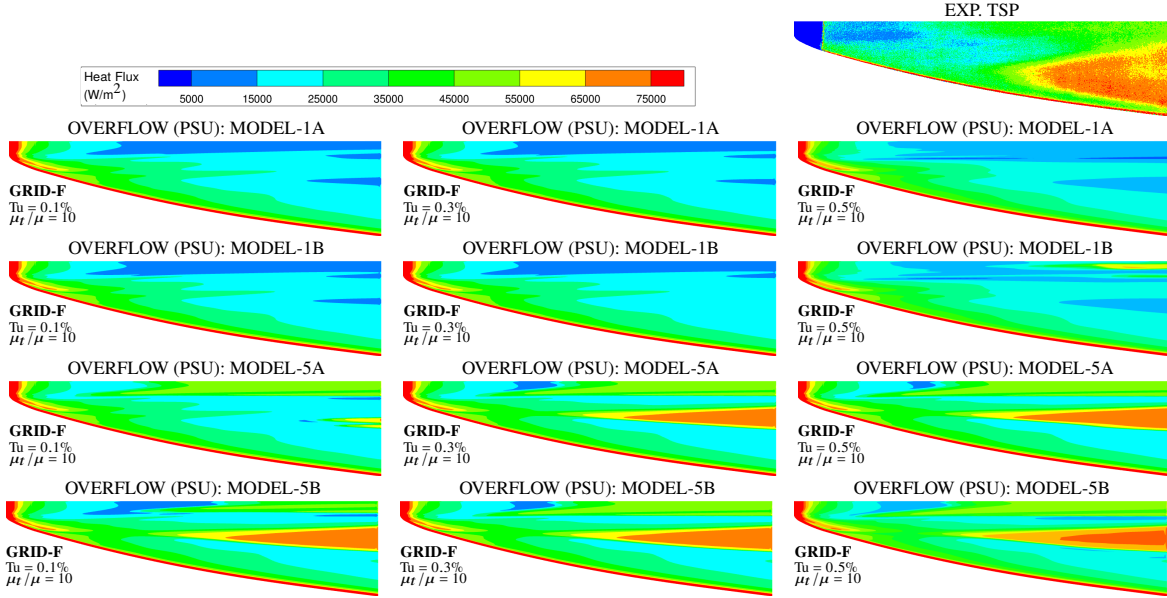
Fig. 14 OVERFLOW (PSU) sensitivity to free-stream turbulent intensity level, GRID-F mesh level. Each row corresponds to a specific model and the turbulent intensity increases from the left to the right
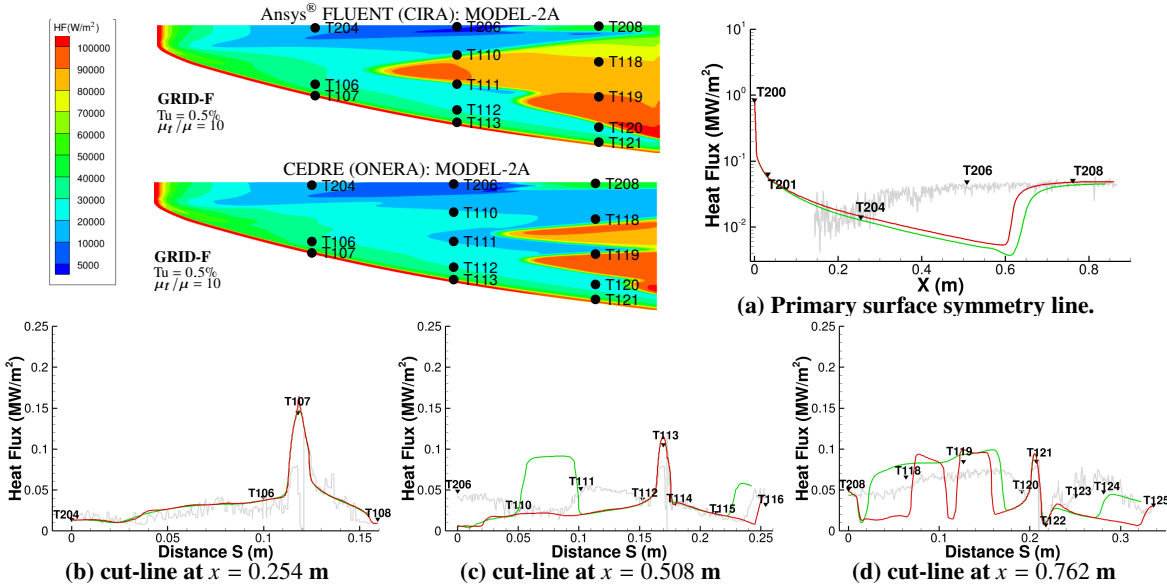

Fig. 15 MODEL-2A, cross-code comparison. TSP ——, Thin films ▼, Ansys® FLUENT® (CIRA) ——, CEDRE (ONERA) ——. Turbulence inlet conditions: $Tu = 0.5\%$, $\mu_t/\mu = 10$. GRID-F mesh level.

discrepancies exist between the outputs of the FLUENT and CEDRE solvers, with FLUENT exhibiting a transition front ahead of that of CEDRE. In the process of comparative analysis, the authors made concerted efforts to minimize the disparities between the codes, focusing on aligning CEDRE with Ansys® FLUENT®. In fact, CEDRE's source files are accessible and amendable, unlike FLUENT, a commercial code with limited possibility for customized source code modifications. Among the differences, the authors identified a discrepancy in the implementation of MODEL-2 which, based on the information in the Ansys® FLUENT® User Guide, appeared to differ in certain coefficients from its original publication [2]. While this modification was incorporated into CEDRE and showed a minimal but not negligible impact on the solutions, it did not eliminate the disparity observed relative to FLUENT.
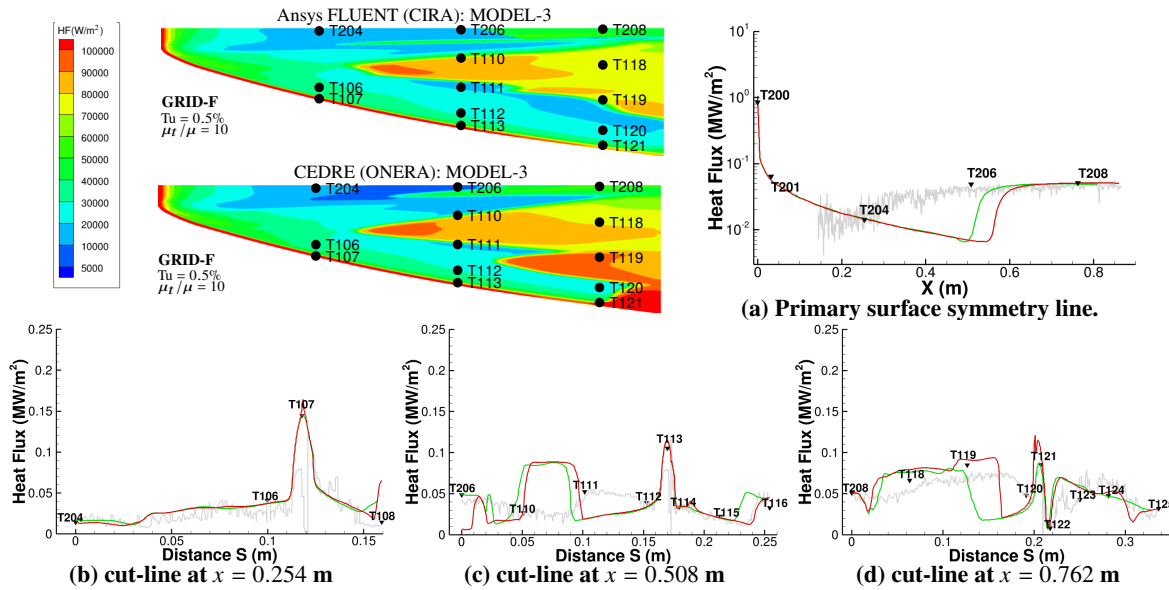
2. Algebraic Model, MODEL-3 (ONERA, CIRA)

(a) Primary surface symmetry line.

(b) cut-line at $x = 0.254$ **m**

(c) cut-line at $x = 0.508$ **m**

(d) cut-line at $x = 0.762$ **m**

Fig. 16   MODEL-3, cross-code comparison. TSP —, Thin films ▾, Ansys® FLUENT® (CIRA) —, CEDRE (ONERA) —. Turbulence inlet conditions: $Tu = 0.5\%$**,** $\mu_t/\mu = 10$**; GRID-F mesh level.**

Figure 16 shows further comparisons between the numerical results obtained from the Ansys® FLUENT® solver (CIRA), and from the CEDRE solver (ONERA). The transition model used here is MODEL-3 recently integrated into the CEDRE solver to enhance its capabilities and enable further comparisons with Ansys® FLUENT®. The comparison was carried out using the finer mesh corresponding to the grid level GRID-F and a freestream turbulence intensity level of $Tu = 0.5\%$.

The transition front based on the wall heat flux demonstrates discernible disparities between the two codes, albeit smaller in contrast to those reported with MODEL-2A. In particular, even though the predictions of the primary lobed shape and the length of the transition front are similar between both solvers, the second and third lobes (the latter being close to the forebody leading edge) are not prominent in the Ansys® FLUENT® solution, contrary to what is seen in the CEDRE data. As mentioned in section VI.B.2, the intense lobe originating near the leading edge is known to be highly mesh dependent and is thus most probably a grid resolution artifact. This confirms that, particularly for this specific transition model, the CEDRE solver demonstrates notable sensitivity to the mesh resolution. It highlights the need for further refinement of the computational mesh to accurately assess the results. The intermediate lobe in the CEDRE data, however, does not originate on the leading edge of the BOLT geometry, is less affected when going towards GRID-M than the third lobe (not shown), and is reminiscent of the one seen with MODEL-2A in the FLUENT data (Figure 15).

3. Hypersonic Transition Model, MODEL-4 (ONERA, NASA)

The two codes that include an implementation of MODEL-4 with and without the cross-flow onset term are CEDRE (ONERA) and OVERFLOW (NASA). In this section, we compare the GRID-F solutions obtained using those two codes for the case with $Tu = 0.3\%$.

As seen in Figure 17, the transition fronts based on the heat flux maps show some discernible differences between the two codes. Looking at the cross-stream cuts along the spanwise distance, the differences between the two codes are apparent along the second and third rows of thin film sensors. But overall, the disagreement is limited to the precise boundary of the transition front while the heat flux values are very similar quantitatively for the laminar and turbulent levels between the two codes. It is interesting to note in Figure 17 that along the symmetry line of the primary surface, neither of the two codes shows a transition onset, while with the addition of the cross-flow onset term, both codes show a transition as seen in Figure 18 for MODEL-4B. The fact that both codes exhibit the same change in behavior along this symmetry line when activating the cross-flow onset term confirms the points raised in section VI.B.1.
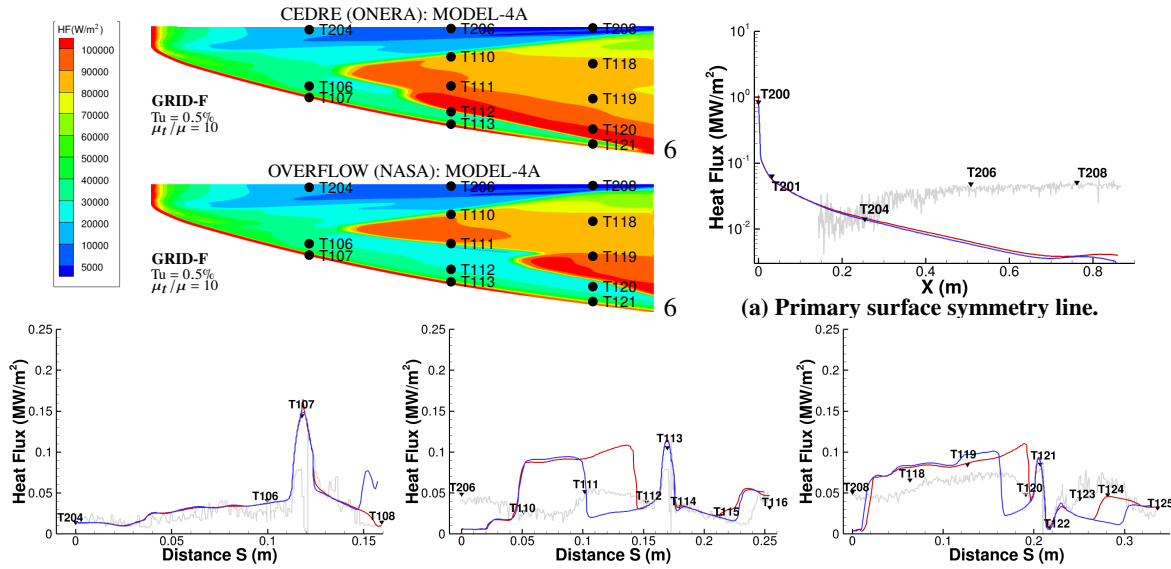
16

Fig. 17 MODEL-4A, cross-code comparison. TSP ——, Thin films ▼, CEDRE (ONERA) ——, OVERFLOW (NASA) ——. Turbulence inlet conditions: $Tu = 0.5\%$, $\mu_t/\mu = 10$; GRID-F mesh level
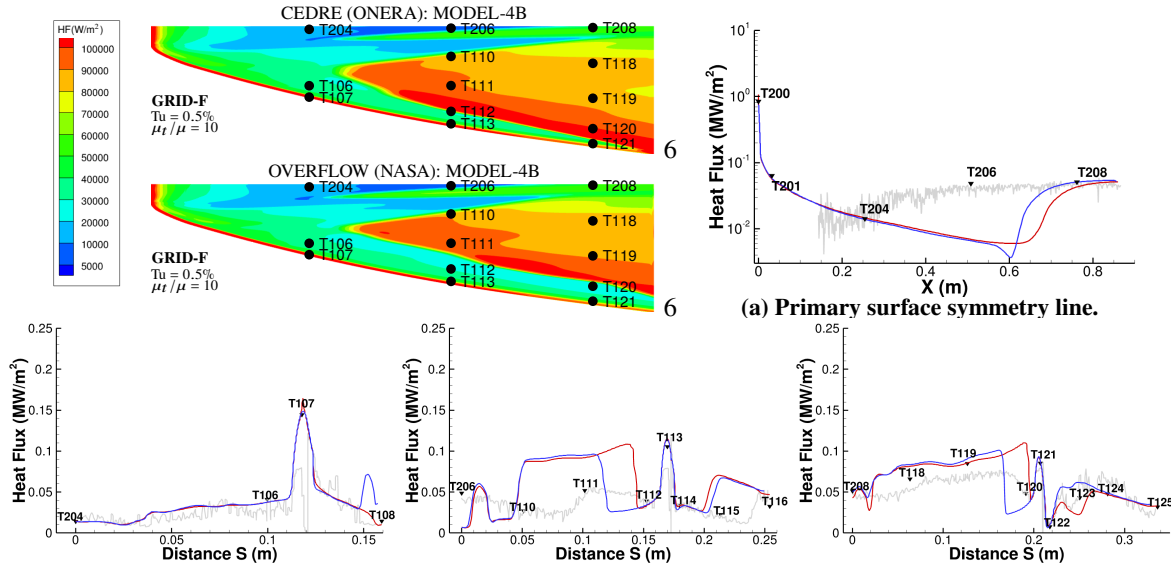

Fig. 18 MODEL-4B, cross-code comparison. TSP ——, Thin films ▼, CEDRE (ONERA) ——, OVERFLOW (NASA) ——: Turbulence inlet conditions: $Tu = 0.5\%$, $\mu_t/\mu = 10$; GRID-F mesh level.

VII. Conclusions

A comparative study of the performance of various transition models has been carried out by computing a common test case that corresponds to a full-scale BOLT model experiment at the CUBRC facility. The transition models, all of which are transport-equation based, are coupled to RANS turbulence models and coded in three different CFD solvers: Ansys® FLUENT®, CEDRE (ONERA), and OVERFLOW (NASA). The majority of these models were developed for transition prediction in low-speed flows, with only one model relying on correlations for Mack second-mode transition. Three models feature onset terms catering for crossflow-induced transition. The present study includes the first assessment of its kind for a complex three-dimensional hypersonic configuration exhibiting multi-mode transition physics.

The sensitivity of the predicted transition front to parameters such as mesh resolution, free-stream turbulence intensity, and viscosity ratios has been thoroughly examined. While nearly all chosen transition models showcased the ability to predict a transition from laminar to turbulent flow in the analyzed test case, the accuracy of these predictions was dependent upon the aforementioned parameters. A noteworthy trend emerged among models incorporating a crossflow correlation, as they successfully predicted transition even at low freestream turbulent intensity levels. In contrast, models lacking this correlation exhibited a stronger sensitivity in the transition front position relative to freestream turbulent intensity level. These findings are consistent with the expectation that the BOLT geometry is one where crossflow-induced transition plays a significant role. The differences in transition predictions evidenced by cross-code comparisons with the same transition model have been carefully analysed and discussed, yet it remains a challenge to attribute such discrepancies (when present) to differences in the underlying numerical methods, to grid resolution effects or to residual modeling discrepancies. The latter is a noteworthy source of potential disparities across results. While a concerted effort has been carried out towards matching precisely the models across codes, the underlying turbulence models diverge from standard formulations in manners that are unique to each code and which could not be altogether reconciled.

Further assessment of these models on additional BOLT tests spanning a broad range of Reynolds numbers and freestream disturbance conditions would be very useful. Future research should also focus on refining these models to better capture complex transition phenomena and to improve the accuracy of predictions whilst being able to determine the associated uncertainties in practical engineering applications.

Acknowledgments

References

[1] Langtry, R. B., and Menter, F. R., "Correlation-Based Transition Modeling for Unstructured Parallelized Computational Fluid Dynamics Codes," *AIAA Journal*, Vol. 47, No. 12, 2009, pp. 2894–2906. https://doi.org/10.2514/1.42362, URL https://doi.org/10.2514/1.42362.

[2] Menter, F. R., Smirnov, P. E., Liu, T., and Avancha, R., "A One-Equation Local Correlation-Based Transition Model," *Flow, Turbulence and Combustion*, Vol. 95, No. 4, 2015, pp. 583–619. https://doi.org/10.1007/s10494-015-9622-4.

[3] Menter, F. R., Matyushenko, A., Lechner, R., Stabnikov, A., and Garbaruk, A., "An Algebraic LCTM Model for Laminar–Turbulent Transition Prediction," *Flow, Turbulence and Combustion*, Vol. 109, No. 4, 2022, pp. 841–869. https://doi.org/10.1007/s10494-022-00336-8.

[4] Cakmakcioglu, S. C., Bas, O., Mura, R., and Kaynak, U., "A revised one-equation transitional model for external aerodynamics," *AIAA Paper 2020-2706*, 2020. https://doi.org/10.2514/6.2020-2706.

[5] Liu, Z., Lu, Y., Li, J., and Yan, C., "Local correlation-based transition model for high-speed flows," *AIAA Journal*, Vol. 60, No. 3, 2022, pp. 1365–1381. https://doi.org/https://doi.org/10.2514/1.J060994.

[6] Qiao, L., Xu, J., Bai, J., and Zhang, Y., "Fully local transition closure model for hypersonic boundary layers considering crossflow effects," *AIAA Journal*, Vol. 59, No. 5, 2021, pp. 1692–1706. https://doi.org/10.2514/1.J059765.

[7] Coder, J. G., and Maughmer, M. D., "Computational Fluid Dynamics Compatible Transition Modeling Using an Amplification Factor Transport Equation," *AIAA Journal*, Vol. 52, No. 11, 2014, pp. 2506-2512. https://doi.org/10.2514/1.J052905.

[8] Carnes, J. A., and Coder, J. G., "Effect of Crossflow Transition on the Pressure-Sensitive-Paint Rotor in Hover," *Journal of Aircraft*, Vol. 59, No. 1, 2022, pp. 29–46. https://doi.org/https://doi.org/10.2514/1.C036121.

[9] Groot, K. J., Patel, J., Saiyasak, C., Coder, J. G., Stefanski, D. L., and Reed, H. L., "Assessment of the Amplification Factor Transport Transition Model for High-Mach Number Flows," *AIAA Paper 2021-2830*, 2021. https://doi.org/10.2514/6.2021-2830.

[10] Berridge, D. C., McKiernan, G., Wadhams, T. P., Holden, M., Wheaton, B. M., Wolf, T. D., and Schneider, S. P., "Hypersonic Ground Tests In Support of the Boundary Layer Transition (BOLT) Flight Experiment," *AIAA Paper 2018-2893*, 2018. https://doi.org/10.2514/6.2018-2893.

[11] Refloch, A., Courbet, B., Murrone, A., Villedieu, P., Laurent, C., Gilbank, P., Troyes, J., Tessé, L., Chaineray, G., Dargaud, J., et al., "CEDRE software," *Aerospace Lab*, 2011, pp. 1–10.

[12] Ansys, Inc., "Fluent," , 2021R1. URL https://www.ansys.com.

[13] Nichols, R. H., and Buning, P. G., *User's Manual for OVERFLOW 2.2*, NASA Langley Research Center, Hampton, VA, August 2010.

[14] Suzen, Y. B., and Huang, P. G., "Modeling of flow transition using an intermittency transport equation," *J. Fluids Eng. – Trans. ASME*, Vol. 122, 2000, pp. 273–284. https://doi.org/https://doi.org/10.1115/1.483255.

[15] Steelant, J., and Dick, E., "Modeling of bypass transition with conditioned Navier–Stokes equations coupled to an intermittency transport equation," *Int. J. Num. Meth. Fluids*, Vol. 23, 1996, pp. 193–220. https://doi.org/https://doi.org/10.1002/(SICI)1097-0363(19960815)23:3<193::AID-FLD415>3.0.CO;2-2.

[16] Menter, F. R., "Two-equation eddy-viscosity turbulence models for engineering applications," *AIAA Journal*, Vol. 32, No. 8, 1994, pp. 1598–1605. https://doi.org/10.2514/3.12149.

[17] Medida, S., and Baeder, J., "Application of the Correlation-based Gamma-Re Theta t Transition Model to the Spalart-Allmaras Turbulence Model," *AIAA Paper 2011-3979*, 2011. https://doi.org/10.2514/6.2011-3979.

[18] Menter, F. R., and Smirnov, P., "Development of a RANS-based Model for Predicting Crossflow Transition," *Proceedings of the contributions to the 19th STAB/DGLR symposium*, 2014.

[19] Arnal, D., Habiballah, M., and Coustols, E., "Théorie de l'instabilité laminaire et critères de transition en écoulement bi et tridimensionnel," *La Recherche aerospatiale*, 1984. URL https://api.semanticscholar.org/CorpusID:171295675.

[20] Spalart, P. R., and Allmaras, S. R., "A One-Equation Turbulence Model for Aerodynamic Flows," *Recherche Aerospatiale*, Vol. 1, 1994, pp. 5–21.

[21] Liou, M. S., "A Further Development of the AUSM+ Scheme Towards Robust and Accurate Solutions for all Speeds," *AIAA Paper 2003-4116*, Orlando, FL, 2003. https://doi.org/https://doi.org/10.2514/6.2003-4116.

[22] Barth, T., and Jespersen, D., "The design and application of upwind schemes on unstructured meshes," *AIAA Paper 89-0366*, 1989. https://doi.org/10.2514/6.1989-366.

[23] Le Touze, C., Murrone, A., and Guillard, H., "Multislope MUSCL method for general unstructured meshes," *Journal of Computational Physics*, Vol. 284, 2015, pp. 389–418. https://doi.org/10.1016/j.jcp.2014.12.032.

[24] Nichols, R. H., and Buning, P. G., *User's Manual for OVERFLOW 2.3*, NASA Langley Research Center, Hampton, VA, August 2010.

[25] Vogel, E., Venkatachari, B. S., and Choudhari, M. M., "Evaluation of Transport-Equation-Based Transition Models for High-Speed Boundary Layers Using OVERFLOW," *AIAA Paper 2023-3531*, 2023. https://doi.org/10.2514/6.2023-3531.

[26] Chan, W. M., III, R. J. G., Rogers, S. E., and Buning, P. G., "Best Practices in Overset Grid Generation," *AIAA Paper 2002-3191*, 2002. https://doi.org/10.2514/6.2002-3191.

[27] Portoni, P., personal communication, 2023.

[28] Wang, L., Xiao, L., and Fu, S., "A modular RANS approach for modeling hypersonic flow transition on a scramjet-forebody configuration," *Aerospace Science and Technology*, Vol. 56, 2016, pp. 112–124. https://doi.org/https://doi.org/10.1016/j.ast.2016.07.004.

[29] Infante, G. M., Cutrone, L., Schettino, A., and Cardone, G., "Numerical methods for laminar-turbulent transition prediction in Hypersonic regime," *2nd International Conference on Flight Vehicles, Aerothermodynamics and Re-entry Missions Engineering (FAR)*, 2023.

[30] Cardesa, J. I., and Delattre, G., "Comparison of RANS transition model predictions on hypersonic three-dimensional forebody configurations," *57th 3AF International Conference on Applied Aerodynamics*, Bordeaux, France, 2023.